Delayed Plastic Relaxation on Patterned Si Substrates: Coherent SiGe Pyramids with Dominant {111} Facets

Zhenyang Zhong,[1,3] W. Schwinger,[1] F. Schäffler,[1] G. Bauer,[1] G. Vastola,[2] F. Montalenti,[2] and L. Miglio[2]
[1]*Institute for Semiconductor and Solid State Physics, Johannes Kepler University Linz, A-4040 Linz, Austria*
[2]*L-NESS and Department of Materials Science, University of Milano Bicocca, Via R. Cozzi 53, 20125 Milano, Italy*
[3]*Surface Physics Laboratory, Fudan University, Shanghai 200433, China*
(Received 7 August 2006; published 23 April 2007)

Unimodal SiGe islands with dominant {111} facets were grown coherently on pit-patterned Si (001) substrates by molecular beam epitaxy. With increasing Ge deposition, the {111} pyramids evolve from dome-shaped islands, reaching significantly larger volumes than are coherently possible on flat substrates. Finite element calculations and molecular dynamics simulations show that SiGe islands in pits can have less misfit strain with respect to islands of the same shape on flat substrates. The injection of dislocations is thus delayed, allowing for the observed development of coherent islands with a very high aspect ratio.

DOI: 10.1103/PhysRevLett.98.176102 PACS numbers: 81.07.−b, 68.37.Lp, 68.37.Ps, 71.15.Pd

Since the first evidence of coherent SiGe island formation [1,2], self-assembled SiGe islands on Si (001) have been extensively studied due to their compatibility with standard Si technology [3]. It is now well established that the evolution of SiGe islands with deposition results from a competition between the relaxation of misfit strain and the increase of the surface energy. After the initial formation of prepyramids [4] or mounds [5], islands bounded by {105} facets appear. They form square-based pyramids, or rectangular-based hut clusters [1], with a height-to-base aspect ratio (a/r) of 0.1. Further volume increase results in multifaceted dome islands with dominant {15, 3, 23} and {113} facets [6–8], and an a/r of about 0.2. The increased average steepness of large islands is attributed to more efficient strain relaxation [9,10]. One would expect an island bounded solely by {111} facets to be the natural evolution at large enough volumes, due to a large steepness combined with a close-packed surface. However, at large volumes, strain relaxation by dislocation injection becomes competitive. Hence, under most experimental conditions, domes are followed by dislocated superdomes [11,12], which show an inverted trend in the a/r vs volume. The formation of coherent islands with a higher a/r than domes has only been reported for SiGe alloys of low Ge content [13–15]. Still, the barn-shaped islands in Refs. [13,15] have a lower a/r than the ones reported here .

In this Letter, we show that a unimodal distribution of coherent SiGe pyramids with dominant {111} facets and $a/r \cong 0.37$ can be realized on patterned Si (001) substrates by solid source MBE. Such {111} pyramids are the result of a shape transition from domes, accompanied by a substantial increase of the a/r. Molecular dynamics (MD) simulations and elasticity-theory calculations are used to explain the role played by the substrate pattern in altering the strain distribution and favoring coherence at high a/r.

Patterned Si(001) substrates with two-dimensionally (2D) periodic pits along two orthogonal ⟨110⟩ directions were obtained by holographic lithography and reactive ion etching [16,17]. To create a well-defined starting surface, a 130 nm thick Si buffer layer was grown with 0.05 nm/s while ramping the temperature from 450 °C to 600 °C. On sample A only the Si buffer was deposited, whereas samples B and C received in addition 5 and 7 monolayers (ML) of Ge, respectively, which were deposited at 620 °C with 0.005 nm/s and 7 s growth interruption after each ML [16]. Associated reference samples on flat substrates, B_f and C_f, were grown simultaneously. The surface morphologies were investigated in air with a Digital Instrument atomic-force microscope (AFM) in the tapping mode. Cross-sectional transmission electron micrographs (XTEM) were taken on a Jeol 2011 FasTEM at 200 keV.

The Si surface morphology before Ge deposition is displayed in Fig. 1(a). It consists of a 2D array of pits that are separated by saddlelike regions. Figures 1(b) and 1(c) show SiGe islands in the center of the pits after deposition of 5 ML (sample B) and 7 ML (sample C) of Ge. Figure 1(d) shows the perfect large scale ordering of the SiGe islands on sample C. Height profiles along the arrows in Figs. 1(b) and 1(c) are shown in Fig. 1(e). On the flat reference substrates, 5 ML of Ge (sample B_f, Fig. 1(f)) lead only to few islands with shapes of hut-clusters (H), pyramids (P), and domes (D), whereas after 7 ML (sample C_f, Fig. 1(g)), randomly distributed domes (height: 17.0(±8.1%) nm, width: 74(±6.0%) nm) are obtained. A few superdomes are also observed.

Most interesting is the evolution of the island shape on the patterned substrates. The islands on sample B are dome-shaped with an octagonal base, whereas the islands on sample C have a quadratic base oriented parallel to the ⟨110⟩ directions and sidewall slope angles of ∼54° (Fig. 1(e)). To analyze the island facets in detail, surface orientation maps (SOM) were extracted, as described in [18]. Figure 2(a) shows the SOM of sample B with dominant {113}, {115}, and {104} facets, which correspond to a state of the island evolution close to domes [6,8], albeit

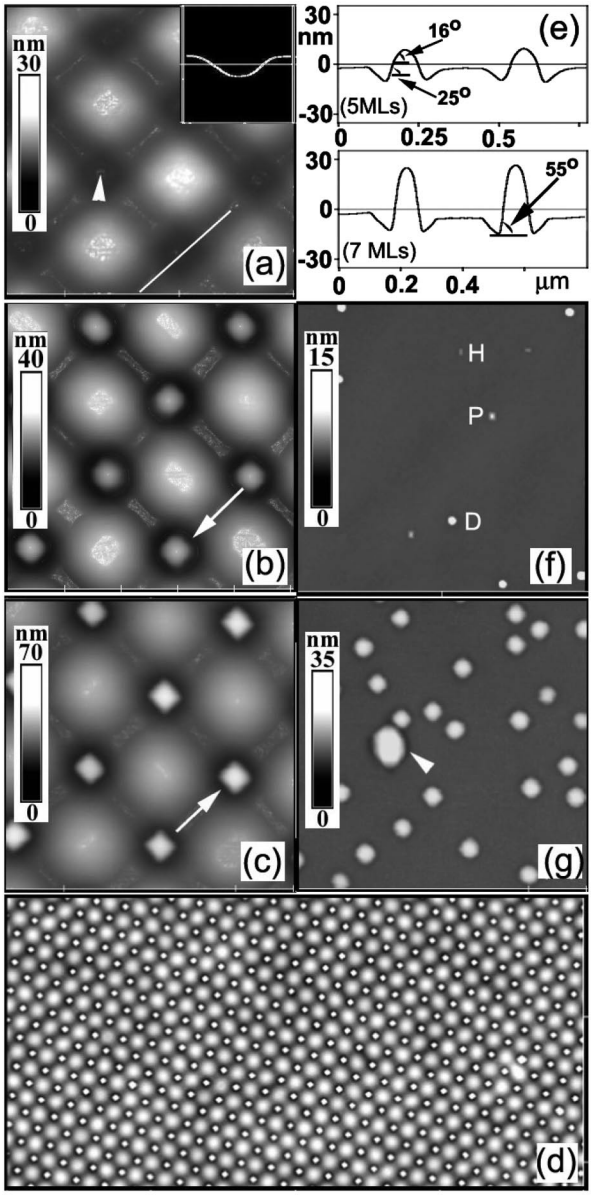

FIG. 1. (a–c) $1 \times 1\ \mu m^2$ AFM images of samples A, B (5 ML Ge), C (7 ML Ge). (d) $10 \times 5\ \mu m^2$ large scale AFM image of sample C. (e) Height profiles of samples B and C along arrows in (b) and (c). (f–g) ($1 \times 1\ \mu m^2$) AFM images of the reference samples B_f (5 ML Ge) and C_f (7 ML Ge) on a flat substrate. The inset in (a) shows a height profile of sample A along the white line with the same vertical scale as in (e); the white triangle in (a) indicates a pit position; "H," "P," and "D" in (f) denote islands with the shapes of hut clusters, {105} pyramids, and domes; the white triangle in (g) indicates a superdome.

with a slightly lower a/r of 0.15. In contrast, the islands on sample C are clearly dominated by the {111} facets (Fig. 2(b)), which occupy ~65% of the total island surface area. {11n} facets with $n > 1$ may appear near the top (Fig. 1(e)), however with much smaller area.

The dominant occurrence of {111} faceted islands on sample C is confirmed by high-resolution XTEM: The resolved (111) lattice planes in Fig. 3(a) are parallel to

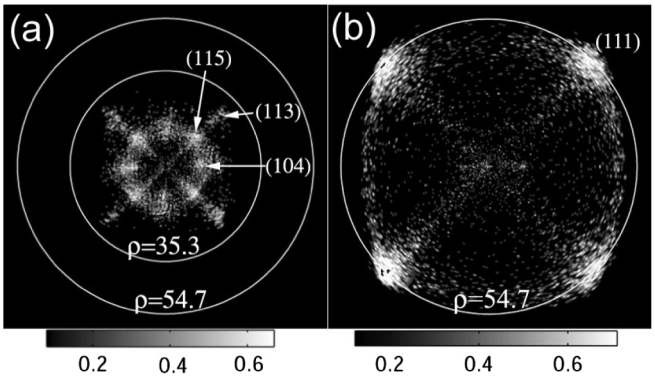

FIG. 2. Surface orientation map of the islands on samples B (a) and C (b). ρ is the inclination angle with respect to [001] and the abscissa corresponds to the [100] azimuth. The gray scale indicates the relative abundance of a specific surface orientation.

the side facet of the island. Moreover, the absence of misfit dislocations in the larger-area XTEM image in Fig. 3(b) demonstrates coherent island growth in the pits.

The islands on sample B can be regarded as precursors to those on sample C. The domes on sample B have a width of 122(±3.3%) nm and a height of 18.7(±7.0%) nm, whereas the {111} pyramids on sample C have a width of 114(±2.0%) nm and a height of 41.9(±4.5%) nm. The dome-to-{111}-pyramid shape transition is thus accompanied by an increase of the island height that enlarges the a/r from 0.15 to 0.37. Although the island base is changed from octagonal to quadratic, its area remains nearly constant during the transition. This requires some rearrangement of the atoms near the base, as has also been observed during the other shape transitions [4,5]. Nevertheless, from an analysis of the scattered x-ray intensity mapped around reciprocal lattice points both in coplanar and grazing incidence diffraction geometry [19], an average Ge composition of about 60% was extracted for the domes on sample B

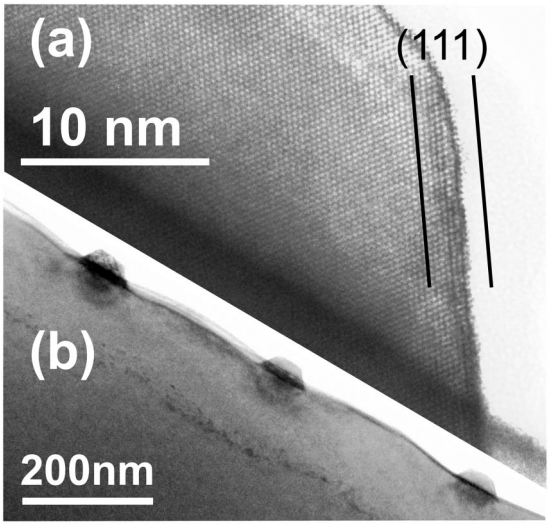

FIG. 3. High-resolution (a) and larger area (b) XTEM image of islands on sample C. The resolved {111} lattice planes in (a) are parallel to the terminating facet (black lines).

as well as the {111} pyramids on sample C [20]. Evidently, the atomic rearrangements do not significantly change the degree of interdiffusion in the islands.

To understand why, in contrast to reported results on flat substrates, {111}-faceted SiGe pyramids can coherently grow on pit-patterned substrates, we calculated the total energy E of coherent islands on both substrate types with respect to a continuous film. We used the simple relation [21] $E = E_R V + E_S S$, where E_R is the relaxation energy per unit volume, E_S the change in the system surface energy due to island formation, V, the total island volume, and S, the change in exposed surface with respect to the flat film. E_R was determined with a Finite Element Method (FEM) software. The evolving shapes were approximated by (i) square-based {105} pyramids with $a/r = 0.1$, (ii) truncated {113} pyramids with $a/r = 0.2$ ("domes"), and (iii) truncated {111} pyramids with $a/r = 0.37$. Average Ge concentrations of $x = 60\%$ and 65% were simulated by imposing the corresponding in-plane misfit strain and linearly interpolating the elastic constants. The surface energies for the reconstructed Ge {001} and {111} surfaces were taken from the *ab initio* calculations in Ref. [22] and a common value of 62.5 meV/Å^2 was used for {105} [23,24] and {1, 1, 10}. From the intersections of the $E(V)$ curves, we evaluated the transition volume from one shape to another on flat and pit-patterned substrates.

FEM and experimental results are compiled in Fig. 4: Panel (a) shows for the flat substrates the data points from sample C_f together with a range of literature data for {105} pyramids (P) [7], as well as domes (D) and superdomes (SD) [25]; cited data refer to growth at 600–620 °C. On the pit-patterned substrate, the data points are from samples B and C, whereas the rectangles represent experimental island volumes from Ref. [26]. Figure 4(b) shows the model predictions for two compositions in either substrate geometry. Experiments and simulations demonstrate that the critical volumes increase substantially from a flat to a pit-patterned substrate, and also, as expected, with decreasing composition. On a flat substrate, the predicted dome-to-{111}-pyramid transition falls into a volume range where dislocated superdomes are found in the experiments; i.e., dislocation formation is here a more efficient route to strain relaxation. In the pit geometry, however, the volume up to which dislocation-free domes can be observed extends significantly into the volume range where dislocated superdomes are present on flat substrates. Furthermore, the experimental volume of the {111} pyramids is consistent with the predictions for $x = 65\%$. We thus conclude that dislocation injection is delayed for growth on pit-patterned substrates.

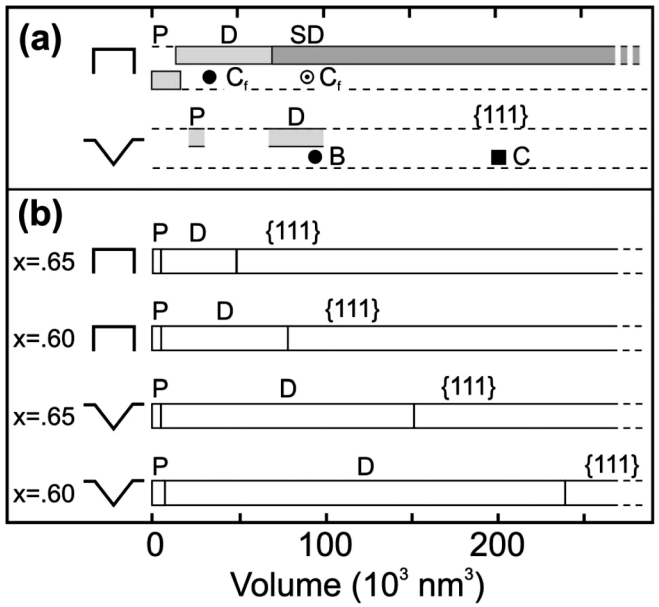

FIG. 4. Island volumes for which {105} pyramids (P), domes (D), and truncated {111} pyramids are stable on flat and pit-patterned substrates; SD denotes dislocated superdomes. (a) Experimental data ranges from Refs. [7,25,26] (gray areas cf. text), and data points from samples C_f, B, and C. (b) FEM simulations for two different Ge concentrations x.

The nucleation of dislocations becomes thermodynamically possible at the critical volume where the energy cost, E_{cost}, for creating a dislocation is equal to the energy gain, ΔE_{gain}, associated with the relief of misfit strain [27]. A lower misfit shifts this critical volume to higher values because ΔE_{gain} is strain-dependent, while E_{cost} is not. To compare the misfit strain both on flat substrates and in pits, we employed MD simulations using the Tersoff potential [28]. For this purpose, we considered quasi two-dimensional Ge{111} pyramids and pits at the scale of 1:10, correctly oriented as in the experiments. The pit sidewalls were assumed as {1, 1, 10} facets, with the initial wetting layer filling one half of the pit depth (5 ML), where it forms a downward pyramid, as sketched in Fig. 5(a). Periodic boundary conditions were applied in the horizontal directions. Each geometry was quenched by a standard MD simulation performed at 0 K, using a time step of 2 fs.

In Fig. 5(a), we plot the elastic energy per Ge atom (i.e., the atomistic counterpart of the E_R term) with respect to the internal layer of a Ge wetting layer. We note that the initial volume of Ge in the pit (downward pyramid) is already partially relaxed and that the Ge in the subsequently forming upward pyramid has lower elastic energy than if it was forming on a flat substrate. The same conclusion holds for the full island in the pit. This behavior can be ascribed to the finding that the in-plane strain component for a downward pyramid is already smaller than the one for a wetting layer. In Fig. 5(b), we plot the in-plane strain ε_{xx} for the second atomic monolayer below the free surface of the downward pyramid. We see that (despite some fluctuations produced by the Si steps in the pit) the value is significantly smaller than the one expected for fully strained Ge on Si (-4.2%). We found that pit-patterning causes a redistribution of the elastic energy between island and substrate. Even with a higher elastic load in the substrate being taken into account, the overall

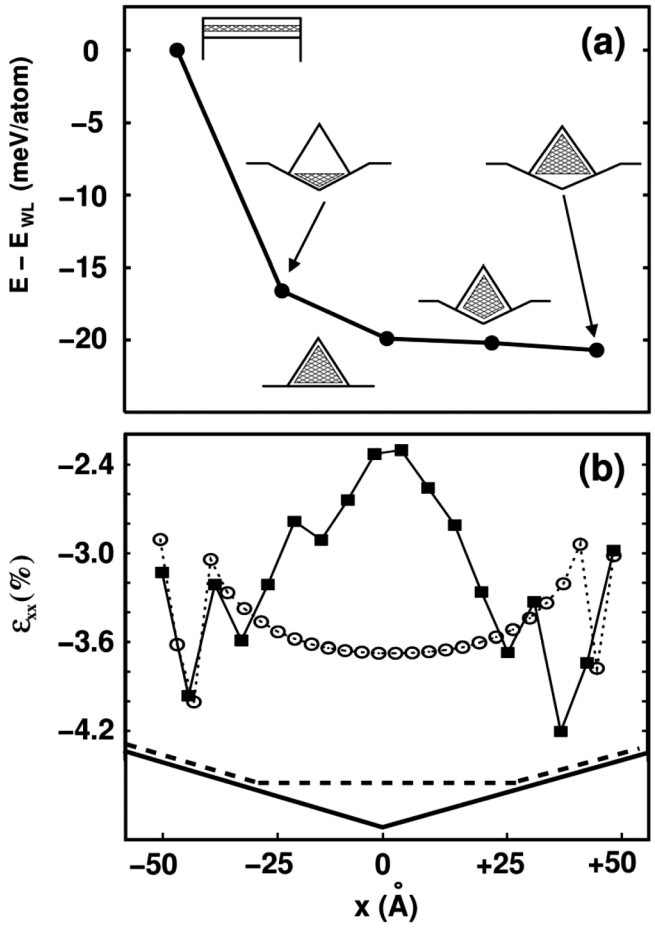

FIG. 5. (a) Elastic energy per atom for the different geometries simulated. From left to right: flat wetting layer, downward pyramid, pyramid on flat substrate, island in pit, upward pyramid. The elastic energy difference per atom between the pyramid on a flat substrate and in the pit is $\cong 0.3$ meV/atom. (b) Horizontal line scan of the ε_{xx} surface strain for a small Ge "cluster" embedded in a V-shaped pit (solid line) and in a trapezoidal-shaped pit (dashed line): In both cases, the surface strain is lower than the misfit strain of a flat Ge wetting layer.

elastic energy of an island inside the pit is still lower than the one for a corresponding island on a flat substrate.

It is worth noting that the pit shape has influence on the strain release in the downward pyramid. If, e.g., the pit is truncated, the strain release at the center of the pit is significantly lower (open circles in Fig. 5(b)). Also, the growth kinetics can be expected to have influence on whether or not the transition from domes to {111} pyramids can be observed. For instance, the less rounded pit geometry in Ref. [29] led to the formation of secondary islands near the upper corners of the pits, which seems to have prevented the central island from reaching the critical volume for the transition to {111} pyramids.

In summary, a shape transition from domes to {111} pyramids was observed with increasing amount of Ge deposition on pit-patterned Si(001) substrates. Elastic-theory and atomistic calculations combined with experimental evidence show that on pit-patterned substrates, the critical volume for dislocation formation can be significantly higher, which is a precondition for the growth of coherent islands with high aspect ratio. Finally, our results indicate that pit-patterned substrates not only provide perfect site control for self-assembled SiGe islands, but can also considerably improve the properties of capped dots [3] due to larger strain relaxation and higher aspect ratios.

This work was supported by FWF (Projects Nos. P16223 and SFB025), and GMe, both Vienna, and by the EU (STREP Project No 012150 and INTAS No. 03-51-5015), Brussels. We thank A. Halilovic for holographic lithography, G. Hesser for TEM preparation, H. Lichtenberger for MBE support, J. Stangl and M. I. Richard for communicating x-ray diffraction results prior to publication, A. Marzegalli and V. A. Zinovyev for helpful discussions.

[1] Y. W. Mo *et al.*, Phys. Rev. Lett. **65**, 1020 (1990).
[2] D. J. Eaglesham and M. Cerullo, Phys. Rev. Lett. **64**, 1943 (1990).
[3] O. G. Schmidt and K. Eberl, IEEE Trans. Electron Devices **48**, 1175 (2001).
[4] A. Vailionis *et al.*, Phys. Rev. Lett. **85**, 3672 (2000).
[5] P. Sutter, P. Zahl, and E. Sutter, Appl. Phys. Lett. **82**, 3454 (2003).
[6] F. M. Ross, R. M. Tromp, and M. C. Reuter, Science **286**, 1931 (1999).
[7] G. Medeiros-Ribeiro *et al.*, Science **279**, 353 (1998).
[8] F. Montalenti *et al.*, Phys. Rev. Lett. **93**, 216102 (2004).
[9] P. Raiteri *et al.*, Phys. Rev. Lett. **88**, 256103 (2002).
[10] C. Liu *et al.*, Phys. Rev. Lett. **84**, 1958 (2000).
[11] T. I. Kamins *et al.*, J. Appl. Phys. **85**, 1159 (1999).
[12] M. De Seta *et al.*, J. Appl. Phys. **92**, 614 (2002).
[13] E. Sutter, P. Sutter, and J. E. Bernard, Appl. Phys. Lett. **84**, 2262 (2004).
[14] W. Dorsch *et al.*, Appl. Phys. Lett. **72**, 179 (1998).
[15] M. Stoffel *et al.*, Phys. Rev. B **74**, 155326 (2006).
[16] Z. Zhong and G. Bauer, Appl. Phys. Lett. **84**, 1922 (2004).
[17] Z. Zhong *et al.*, J. Appl. Phys. **93**, 6258 (2003).
[18] Z. Zhong *et al.*, Physica E (Amsterdam) **23**, 243 (2004).
[19] T. U. Schülli *et al.*, Appl. Phys. Lett. **89**, 143114 (2006).
[20] For details on the determination of the Ge composition gradient, see M.-I. Richard *et al.* (to be published).
[21] J. Tersoff and F. K. LeGoues, Phys. Rev. Lett. **72**, 3570 (1994).
[22] A. A. Stekolnikov and F. Bechstedt, Phys. Rev. B **72**, 125326 (2005).
[23] D. B. Migas *et al.*, Surf. Sci. **556**, 121 (2004).
[24] O. E. Shklyaev *et al.*, Phys. Rev. Lett. **94**, 176102 (2005).
[25] T. Merdzhanova *et al.*, Phys. Rev. Lett. **96**, 226103 (2006).
[26] G. Chen *et al.*, Phys. Rev. B **74**, 035302 (2006).
[27] K. Tillmann and A. Förster, Thin Solid Films **368**, 93 (2000).
[28] J. Tersoff, Phys. Rev. B **39**, 5566 (1989).
[29] Z. Zhong, O. G. Schmidt, and G. Bauer, Appl. Phys. Lett. **87**, 133111 (2005).